Mechanistic Aspects of Ethylene Polymerization by Iron(II)−Bisimine Pyridine Catalysts: A Combined Density Functional Theory and Molecular Mechanics Study

Liqun Deng, Peter Margl, and Tom Ziegler*

Contribution from the Department of Chemistry, The University of Calgary, Calgary, Alberta T2N 1N4, Canada

Received December 21, 1998. Revised Manuscript Received May 6, 1999

Abstract: We present an extensive theoretical study of the iron(II)−bisimine pyridine based ethylene-polymerization catalysts $\{[2,6\text{-}((R)N{=}C(R'))_2{-}C_5H_3N]FeC_3H_7\}^+$ (R = R′ = H, **1a**; R = 2,6-C_6H_4(i-Pr)$_2$, R′ = CH_3, **1A**) recently developed by the groups of Brookhart and Gibson. The study was based on density functional theory (DFT) for the "generic" model system **1a** and a combined DFT and molecular mechanics approach for the "real" system **1A**. It is shown that the rate-determining step for both termination and propagation in the "real" system is the capture of ethylene by **1A**. The steric bulk introduced by R = 2,6-C_6H_4(i-Pr)$_2$ was found to suppress ethylene capture for the termination step and increase the rate of insertion. Termination takes place on the singlet potential energy surface (PES). For propagation the singlet and triplet PES's are close in energy and spin-state change is possible. The quintet states are too high in energy to play any role in polymerization. The model system **1a** was found to form an ethylene complex that is too stable for any further chemical transformation to take place.

Introduction

There is currently considerable interest in the development of new and versatile metal-based olefin polymerization catalysts.[1−6] Quite recently the groups of Brookhart[7] and Gibson[8] have investigated the catalytic potential of iron(II) and cobalt-(II) complexes with tridentate pyridine bisimine ligands (Scheme 1). They find that especially the iron(II) system can produce high-density polyethylene in good yields when bulky ortho-substituted aryl groups are attached to the imine nitrogens. The new catalysts have polymerization activities comparable to, or even higher than, those of metallocenes under similar conditions. They exhibit further great potential for controlling polymer properties by external parameters such as pressure and temperature.

More established polymerization catalysts have been the subjects of numerous mechanistic studies based on experimental[9−11] and theoretical techniques.[12−23] It is the objective of the present computational study to extend our mechanistic knowledge of polymerization to the new type of Fe(II)-based catalysts. A corresponding detailed experimental investigation has not yet been published.

Scheme 1. Real and Generic Catalytic Systems

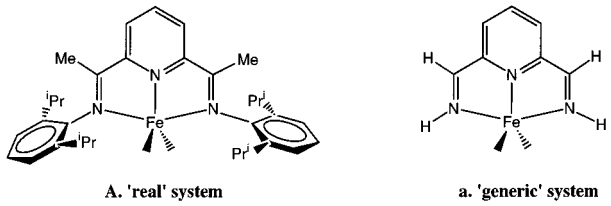

A. 'real' system **a. 'generic' system**

(1) Brintzinger, H. H.; Fischer, D.; Mülhaupt, R.; Rieger, B.; Waymouth, R. M. *Angew. Chem., Int. Ed. Engl.* **1995**, *34*, 1143.
(2) Bochmann, M. *J. Chem. Soc., Dalton Trans.* **1996**, 255.
(3) Fink, G.; Muelhaupt, R.; Brintzinger, H. H. *Ziegler Catalysts: Recent Scientific Innovations and Technological Improvement*; Springer-Verlag: Berlin, 1995.
(4) Coates, G. W.; Waymouth, R. M. In *Comprehensive Organometallic Chemistry II*; Abel, E. W., Stone, F. G. A., Wilkinson, G., Eds.; Pergamon Press: New York,1995; Vol. 12, p 1193.
(5) Yang, X.; Stern, C. L.; Marks, T. *J. Am. Chem. Soc.* **1994**, *116*, 10015.
(6) Freemantle, M. *Chem. Eng. News* **1998**, *76*, 11.
(7) (a) Small, B. L.; Brookhart, M.; Bennett, A. M. A. *J. Am. Chem. Soc.* **1998**, *120*, 4049. (b) Small, B. L.; Brookhart, M. *J. Am. Chem. Soc.* **1998**, *120*, 7143.
(8) Britovsek, G. J. P.; Gibson, V. C.; Kimberly, B. S.; Maddox, P. J.; McTavish, S. J.; Solan, G. A.; White, A. J. P.; Williams, D. J. *Chem. Commun.* **1998**, 849.
(9) Johnson, L. K.; Killian, C. M.; Brookhart, M. *J. Am. Chem. Soc.* **1995**, *117*, 6414.
(10) Johnson, L. K.; Mecking, S.; Brookhart, M. *J. Am. Chem. Soc.* **1996**, *118*, 267.
(11) Resconi, L.; Piemontesi, F.; Camurati, I.; Sudmeijer, O.; Nifant'ev, I. E.; Ivchenko, P. V.; Kuz′mina, L. G. *J. Am. Chem. Soc.* **1998**, *120*, 2308.
(12) Jolly, C. A.; Marynick, D. S. *J. Am. Chem. Soc.* **1989**, *111*, 7968.
(13) Castonguay, L. A.; Rappé, A. K. *J. Am. Chem. Soc.* **1992**, *114*, 5832.
(14) Kawamura-Kuribayashi, H.; Koga, N.; Morokuma, K. *J. Am. Chem. Soc.* **1992**, *114*, 2359, 8687.
(15) Weiss, H.; Ehrig, C.; Ahlrichs, R. *J. Am. Chem. Soc.* **1994**, *116*, 4919.
(16) Bierwagen, Erik P.; Bercaw, John E.; Goddard, W. A., III *J. Am. Chem. Soc.* **1994**, *116*, 1481.
(17) Woo, T. K.; Fan, L.; Ziegler, T. *Organometallics* **1994**, *13*, 2252.
(18) Yoshida, T.; Koga, N.; Morokuma, K. *Organometallics* **1995**, *14*, 746
(19) Das, P. K.; Dockter, D. W.; Fahey, D. R.; Lauffer, D. E.; Hawkins, G. D.; Li, J.; Zhu, T.; Cramer, C. J.; Truhlar, D. G.; Dapprich, S.; Froese, R. D. J.; Holthausen, M. C.; Liu, Z.; Mogi, K.; Vyboishchikov, S.; Musaev, D. G.; Morokuma, K. *ACS Symp. Ser.* **1999**, *721*, 208.
(20) Margl, P.; Deng, L.; Ziegler, T. *J. Am. Chem. Soc.* **1998**, *120*, 5517.
(21) Deng, L.; Ziegler, T.; Woo, T. K.; Margl, P.; Fan, L. *Organometallics* **1998**, *17*, 3240.
(22) Froese, R. D. J.; Musaev, D. G.; Morokuma, K. *J. Am. Chem. Soc.* **1998**, *120*, 1581.
(23) Musaev, D. G.; Froese, R. D. J.; Morokuma, K. *Organometallics* **1998**, *17*, 1850.

10.1021/ja984385l CCC: $18.00
Published on Web 06/19/1999

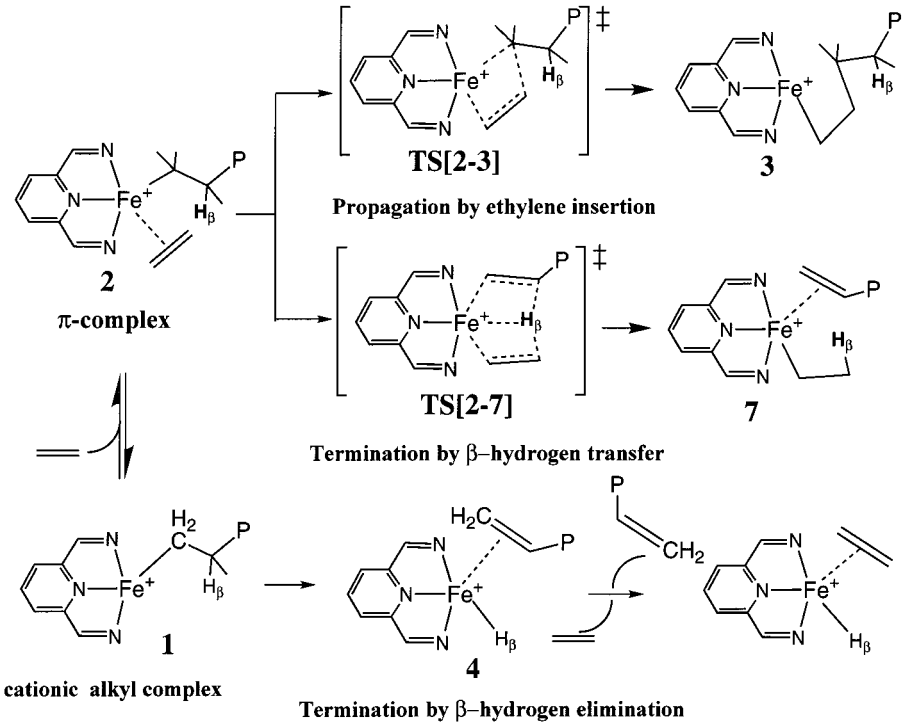

Figure 1. A schematic representation of the elementary reaction steps in ethylene polymerization catalyzed by iron(II)−bisimino pyridine complexes.

We shall in our theoretical study assume that the active Fe(II) species is a cationic metal−alkyl complex **1** (Figure 1) by analogy to other olefin catalysts.[1,5,10,24−25] The elementary reaction steps under investigation will in the first place involve ethylene uptake by **1** to form an iron(II)−alkyl ethylene π-complex **2** (Figure 1) as well as insertion of the coordinated ethylene into the Fe−C_α(alkyl) bond (chain propagation). We shall in addition consider chain termination (transfer) that might occur via unimolecular β-H elimination (BHE) or by way of bimolecular β-H transfer (BHT), Figure 1. The latter process can proceed either in a fully concerted fashion, as predicted by previous theoretical studies,[21,30] or in a multistep associative mechanism, as suggested by Johnson et al.[10] in a study of their Ni(II) and Pd(II) diimine-based catalysts.

Computational Models and Methods

Models. The actual Brookhart/Gibson catalyst $\{[2,6\text{-}((R)N{=}C(R'))_2{-}C_5H_3N]FeC_3H_7\}^+$ ($R = 2,6\text{-}C_6H_4(i\text{-}Pr)_2$, $R' = CH_3$) carries bulky phenyl substituents, **1A** of Scheme 1. We have in the first place investigated a simplified model $\{[2,6\text{-}(HN{=}CH)_2{-}C_5H_3N]FeC_3H_7\}^+$ of the Brookhart/Gibson catalyst in which the phenyl and methyl substituents are replaced by hydrogens, **1a** of Scheme 1. This model should provide important information about the electronic properties of the Fe(II) catalyst and will subsequently be referred to as the "generic" system. Calculations will also be carried out on the actual Brookhart/Gibson Fe(II) catalyst that we shall refer to as the "real" system. A comparison between calculations on the "real" and "generic" systems should provide information about the role played by the phenyl and methyl substituents in Scheme 1A. The "generic" system was treated by quantum mechanical (QM) density functional theory based methods (DFT) whereas a combined quantum mechanics and molecular mechanics (QM/MM) approach was applied to the "real" system. Solvent and counterion effects were not included in our calculations. A justification for neglecting these effects has been given in previous papers.[21,30]

Density Functional Theory (DFT) Methods. All reported DFT calculations were performed by means of the Amsterdam Density Functional (ADF) program system.[31−35] The electronic configurations of the molecular systems were described by a triple-ζ basis set[36,37] on the iron center for the 3s, 3p, 3d, 4s, and 4p valence shells. A double-ζ STO basis set was used for carbon (2s, 2p), hydrogen (1s), and nitrogen (2s, 2p), augmented with a single 3d polarization function except for hydrogen where a 2p function was used. The inner shells on the metals as well as carbon and nitrogen were treated within the frozen core approximation. A set of auxiliary[38] s, p, d, f, and g STO functions, centered on all nuclei, was used to fit the molecular density and present Coulomb and exchange potentials accurately in each SCF cycle. Energy differences were calculated by augmenting the local exchange−correlation potential by Vosko[39] et al. with Becke's[40] nonlocal exchange corrections and Perdew's[41,42] nonlocal correlation corrections (BP86) in a self-consistent manner. Geometries were optimized at the same level. First-order (FO) scalar relativistic corrections[43,44] were added to the total energy.

(24) Jordan, R. F. *Adv. Organomet. Chem.* **1991**, *32*, 325.
(25) Scollard, J. D.; McConville, D. H. *J. Am. Chem. Soc.* **1996**, *118*, 10008.
(26) Lohrenz, J. C. W.; Woo, T. K.; Ziegler, T. *J. Am. Chem. Soc.* **1995**, *117*, 12793.
(27) Woo, T. K.; Margl, P. M.; Lohrenz, J. C. W.; Blöchl, P. E.; Ziegler, T. *J. Am. Chem. Soc.* **1996**, *118*, 13021.
(28) Margl, P.; Deng, L.; Ziegler, T. *J. Am. Chem. Soc.* **1999**, *121*, 154.
(29) Deng, L.; Margl, P. M.; Ziegler, T. *J. Am. Chem. Soc.* **1997**, *119*, 1094.
(30) Deng, L.; Woo, T. K.; Cavallo, L.; Margl, P. M.; Ziegler, T. *J. Am. Chem. Soc.* **1997**, *119*, 6177.
(31) Baerends, E. J.; Ellis, D. E.; Ros, P. *Chem. Phys.* **1973**, *2*, 41.
(32) Baerends, E. J.; Ros, P. *Chem. Phys.* **1973**, *2*, 52.
(33) Ravenek, W. In *Algorithms and Applications on Vector and Parallel Computers*; t. Riele, H. J. J., Dekker, T. J., v. d. Horst, H. A., Eds.; Elsevier: Amsterdam, The Netherlands, 1987.
(34) te Velde, G.; Baerends, E. J. *J. Comput. Chem.* **1992**, *99*, 84.
(35) Versluis, L.; Ziegler, T. *J. Chem. Phys.* **1988**, *88*, 322.
(36) Snijders, J. G.; Baerends, E. J.; Vernoijs, P. *At. Nucl. Data Tables* **1982**, *26*, 483.
(37) Vernoijs, P.; Snijders, J. G.; Baerends, E. J. *Slater Type Basis Functions for the Whole Periodic System*; Department of Theoretical Chemistry, Free University: Amsterdam, The Netherlands, 1981.
(38) Krijn, J.; Baerends, E. J. *Fit Functions in the HFS Method*; Department of Theoretical Chemistry, Free University: Amsterdam, The Netherlands, 1984.
(39) Vosko, S. H.; Wilk, L.; Nusair, M. *Can. J. Phys.* **1980**, *58*, 1200.
(40) Becke, A. *Phys. Rev. A* **1988**, *38*, 3098.
(41) Perdew, J. P. *Phys. Rev. B* **1986**, *33*, 8822.
(42) Perdew, J. P. *Phys. Rev. B* **1986**, *34*, 7406.

We have previously shown that the DFT method is able to reproduce experiential activation barriers to within 2−5 kcal/mol for olefin or carbonyl insertion into the metal−carbon bond.[30,45−47,51] Metal−ligand dissociation energies have been shown to be correct to within 5 kcal/mol.[48−52] Similar conclusions have been drawn by Robb et al.[53] in their study of the nickel−olefin complexes, and more recently by Jensen and Børve[54] in their systematic study of the titanium-based Ziegler−Natta catalyst system.

Combined DFT and Molecular Mechanics (MM) Scheme. The ADF program system was modified[55] to include the AMBER95[56] molecular mechanics force field. In addition, the QM(DFT) and MM parts were coupled self-consistently according to the method prescribed by Maseras and Morokuma.[57] In the combined QM/MM calculations, the QM part consisted of the generic complex (Scheme 1a) in which the substituents on the nitrogen atoms were replaced by hydrogen atoms. The actual bulky aryl groups attached to the nitrogens were treated by the pure MM method. The QM and MM parts were linked by the "dummy" hydrogen atoms and coupled by van der Waals interactions. The geometry optimization on the entire system was carried out with coupling between QM and MM atoms.[55] In the optimization of the MM part the N−C(aryl) and C−C(methyl) distances were constrained to be 0.412 and 0.4368 Å longer than the optimized N−H and C−H distances so as to fit the experimental C−C bond lengths. An augmented AMBER95[56] force field was utilized to describe the molecular mechanics potential except for the van der Waals parameter of the iron atom, for which Rappé's universal force field (UFF)[58] was employed. All force field parameters are provided as Supporting Information. Electrostatic interactions were not included in the molecular mechanics potential. A similar approach has been applied successfully in a previous[30] study of the Brookhart Ni(II)−diimine system.

Stationary Points. All reported energy minimum points and transition states were fully optimized with convergence criteria of the maximum and rms gradient being less than 0.001 and 0.0006 au, respectively. Energy changes upon tightening the convergence criteria proved to be within a couple of tenths of a kilocalorie/mole.

Labeling of the Molecules. A number of labeling conventions have been adopted throughout this paper. Thus, species of the generic system will be referred to by numerals attached to lower-case letters (e.g., **1a**, **1b**, **1c**), whereas numerals attached to upper-case letters (e.g., **2A**, **1B**, **3C**) refer to structures of the "real" system. Further, the numeric-alphabetic labels may have the postfix (t) or (q) for species with respectively a triplet and quintet spin state. On the other hand, labels without the postfix refer to species with a singlet spin state. All transition states have the prefix TS followed by the direct (kinetic) reactant and product within square brackets. Finally, "real" and "generic" systems with the same numeric-alphabetic label represent analogous species with the same conformation at the metal center.

Results and Discussion

We shall start our investigation by probing the potential energy surface (PES) of the "generic" model for the Brookhart/Gibson catalyst (Scheme 1a). The role of the bulky substituents will be analyzed in a subsequent discussion of the "real" system (Scheme 1A).

Table 1. Relative Energies (kcal/mol) of the Stationary Points on the Singlet Potential Energy Surface for the "Generic" Brookhart/Gibson Model Catalyst (Scheme 1a)

category	description	species[a]	energy[a]	barrier[b]
alkyl complex + C_2H_4	ax β-agostic	**1a**	0.0	
	ax nonagostic	**1b**	10.9	
	eq β-agostic	**1c**	11.5	
	eq nonagostic	**1d(t)**	6.6	
π-complexes	FS ax β-agostic	**2a**	−29.7	
	FS ax nonagostic	**2b**	−21.1	
	BS eq β-agostic	**2c**	−23.8	
	FS eq nonagostic	**2d**	−14.8	
	BS capture TS	**TS[1a−2c](t)**	6.1	6.1
	2a−**2c** conversion	**TS[2a−2c](t)**	−6.7	23.0
insertion TS	BS insertion TS	**TS[2c−3c]**	−16.4	7.4
	ax alkyl TS	**TS[2b−3b]**	16.2	37.3
	FS insertion TS	**TS[2d−3d]**	−13.9	0.9
insertion products	β-agostic	**3a**	−25.5	
	γ-agostic	**3d**	−24.3	
	δ-agostic	**3c**	−24.4	
	δ-β conversion TS	**TS[3c−3a]**	−21.8	2.6
	γ-β conversion TS	**TS[3d−3a]**	−16.9	7.4
β-H elimination + C_2H_4	transition state	**TS[1a−4a]**	11.4	11.4
	product	**4a**	1.2	
	chain-ejection prod	**5a** + C_3H_6	38.1	38.1
	7a isomerizn TS	**TS[4a−6a]**	7.0	5.8
	1a's isomer LFe^iPr^+	**6a**	−1.5	−2.7
β-H transfer	transition state	**TS[2a−7a]**	−25.7	4.0
	product	**7a**	−30.9	
	chain-ejection prod	**8a** + C_3H_6	−1.8	
	5a isomerizn TS	**TS[7a−9a]**	−27.6	3.3
	5a isomerizn prod	**9a**	−32.4	
	β-H transfer TS	**TS[9a−10a]**	−26.6	5.8
	2a's isomer $LFe^iPrC_2H_4^+$	**10a**	−30.5	

[a] **1d(t)**, **TS[1a−2c](t),** and **TS[2a−2c](t)** lie on the triplet PES. [b] Energies relative to **1a** + C_2H_4. [c] Reaction barrier relative to the direct precursor.

A. Generic System. Calculations at the BP86 level of theory reveal that the energy minimum paths for the catalytic reaction steps primarily are confined to the singlet PES. Table 1 summarizes the energetics of key stationary points along the reaction paths. Figure 2 plots the energy profile for the most feasible chain propagation, termination, and isomerization reaction steps. Also depicted in Figure 2 are the conformations of the involved species along the reaction paths. All optimized structures are provided as Supporting Information.

i. Iron(II) Alkyl Complexes. The Fe(II)−alkyl complex can adopt an "axial" conformation with the C_α atom nearly perpendicular to the iron−nitrogen coordination plane. The most stable "axial" conformation has a β-H agostic bond (**1a**). Rupture of the agostic bond leads to the "axial" conformation **1b** that is 10.9 kcal/mol higher in energy. The Fe(II)−alkyl complex might alternatively adopt an "equatorial" conformation with the C_α atom in the Fe(II) coordination plane (**1c**). The "equatorial" structure **1c** is unfavorable by 11.5 kcal/mol compared to **1a** as the C_α atom in **1c** is destabilized by the trans interaction from the pyridine ligand. Further, the H_β of **1c** almost eliminates to the metal center with the $C_\beta-H_\beta$ bond length of 1.40 Å due to strong interaction between the 1s orbital of the H_β and the d_{z^2} orbital of the metal. Frequency calculation shows that **1c** has an imaginary frequency (153i) corresponding to the $C_\beta-H_\beta$ stretching. Hence **1c** is a transition state in nature.

ii. Iron(II)−Alkyl Ethylene Complexes. We have located four alkyl ethylene complexes on the PES. Of lowest energy is **2a** that is formed by syn (frontside) addition of ethylene to the

(43) Snijders, J. G.; Baerends, E. J. *Mol. Phys.* **1978**, *36*, 1789.
(44) Snijders, J. G.; Baerends, E. J.; Ros, P. *Mol. Phys.* **1979**, *38*, 1909.
(45) Margl, P.; Ziegler, T. *Organometallics* **1996**, *15*, 5519.
(46) Margl, P. M.; Ziegler, T. *J. Am. Chem. Soc.* **1996**, *118*, 7337.
(47) Stanton, R. V.; Merz, K. M. J. *J. Chem. Phys.* **1993**, *100*, 434.
(48) Folga, E.; Ziegler, T. *J. Am. Chem. Soc.* **1993**, *115*, 5169.
(49) Li, J.; Schreckenbach, G.; Ziegler, T. *J. Phys. Chem.* **1994**, *98*, 4838.
(50) Li, J.; Schreckenbach, G.; Ziegler, T. *J. Am. Chem. Soc.* **1995**, *117*, 486.
(51) Ziegler, T.; Li, J. *Can. J. Chem.* **1994**, *72*, 783.
(52) Ziegler, T.; Li, J.; Schreckenbach, G. *Inorg. Chem.* **1995**, *34*, 3245.
(53) Bernardi, F.; Bottoni, A.; Calcinari, M.; Rossi, I.; Robb, M. A. *J. Phys. Chem. A.* **1997**, *101*, 6310.
(54) Jensen, V. R.; Børve, K. J. *J. Comput. Chem.* **1998**, *19*, 947.
(55) Woo, T. K.; Cavallo, L.; Ziegler, T. *Theor. Chem. Acc.* **1998**, accepted for publication.
(56) Cornell, W. D.; Cieplak, P.; Bayly, C. I.; Gould, I. R.; Merz, K. M. Jr.: Ferguson, D. M.; Spellmeyer, D. C.; Fox, T.; Caldwell, J. W.; Kollman, P. A. *J. Am. Chem. Soc.* **1995**, *117*, 5179.
(57) Maseras, F.; Morokuma, K. *J. Comput. Chem.* **1995**, *16*, 1170.
(58) Rappé, A. K.; Casewit, C. J.; Colwell, K. S.; Goddard, W. A., III; Skiff, W. M. *J. Am. Chem. Soc.* **1992**, *114*, 10024.

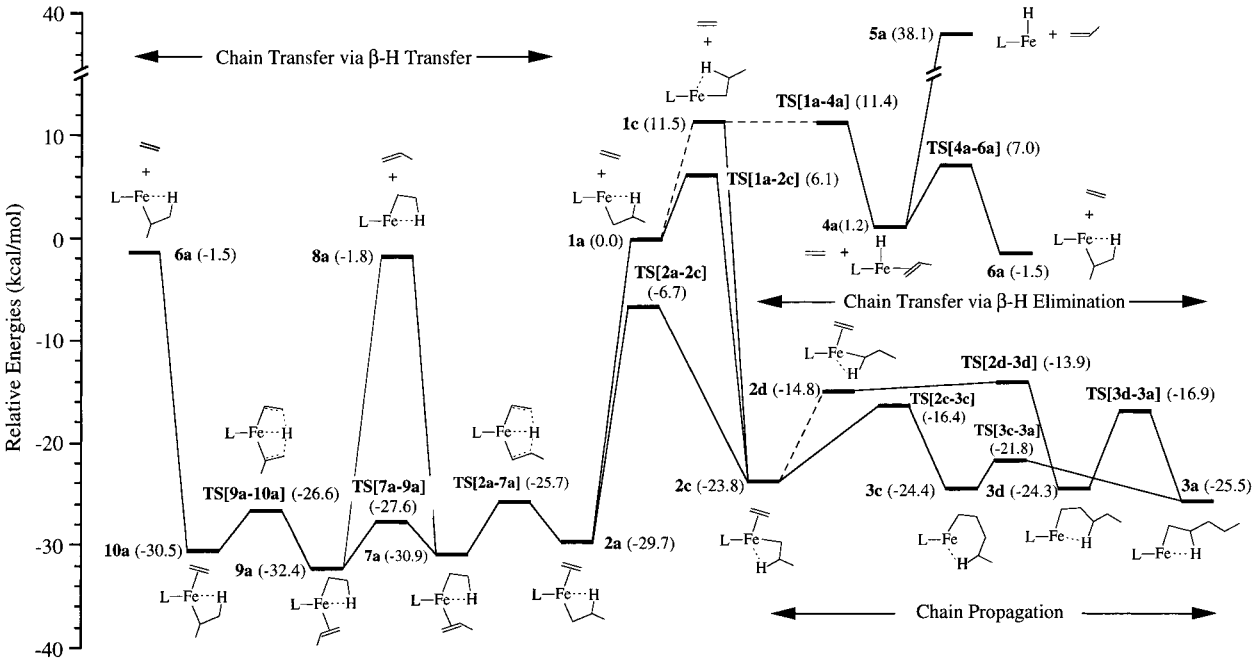

Figure 2. Singlet potential energy surface for the "generic" model system. TS[**1a**−**2c**](t) and TS[**2a**−**2c**](t) are situated on the triplet surface. Note that the iron−nitrogen coordination plane is perpendicular to the paper.

Scheme 2. Four Conformations of the Iron(II)−Alkyl Complexes

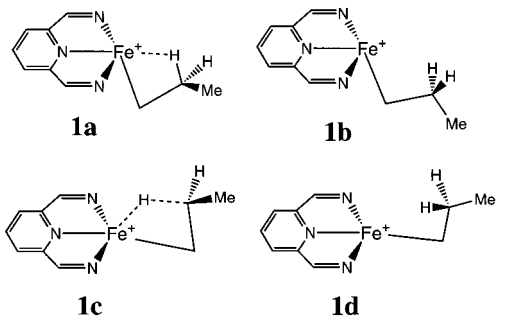

β-agostic bond of the most stable alkyl complex **1a** in a path from above the iron−nitrogen plane trans to the C_α atom. The agostic bond is retained in **2a** and ethylene is complexed by 29.7 kcal/mol. Complexation of ethylene to the less stable "axial" alkyl complex **1b** results in **2b** that is 8.6 kcal/mol higher in energy than **2a**, primarily due to the lack of an agostic bond. Uptake of ethylene anti to the agostic bond (backside) of the "equatorial" alkyl complex **1c** leads to **2c** that is 5.9 kcal/mol less stable than **2a** due to the position of C_α in the equatorial plane. Capture of an ethylene by **1a**, **1b**, and **1c** to form **2a**, **2b**, and **2c**, respectively, proceeds without an enthalpic barrier.

The two ethylene complexes **2a** and **2c** with β-hydrogen agostic bonds can be considered to have an octahedral coordination around the metal with the β-hydrogen as the sixth ligand. The d levels are accordingly split into a set of three "t_{2g}" orbitals (d_{xy}, d_{xz}, and d_{yz}) and two "e_g" levels (d_{z^2} and $d_{x^2-y^2}$), Figure 3, with a sufficiently large splitting to afford a low-spin t_{2g}^6 singlet. The occupied π-orbital of ethylene is seen to have a good overlap with the empty d_{z^2} orbital, Figure 3, on the metal center. This interaction is primarily responsible for the strong ethylene−Fe(II) bond of 29.7 kcal/mol in **2a**.

The direct interconversion of the C_α atom from the axial, **2a**, to the equatorial, **2c**, position is associated with a considerable kinetic barrier since the occupied sp^3 σ-orbital on the C_α atom will begin to interact and destabilize the occupied d_{xz} metal

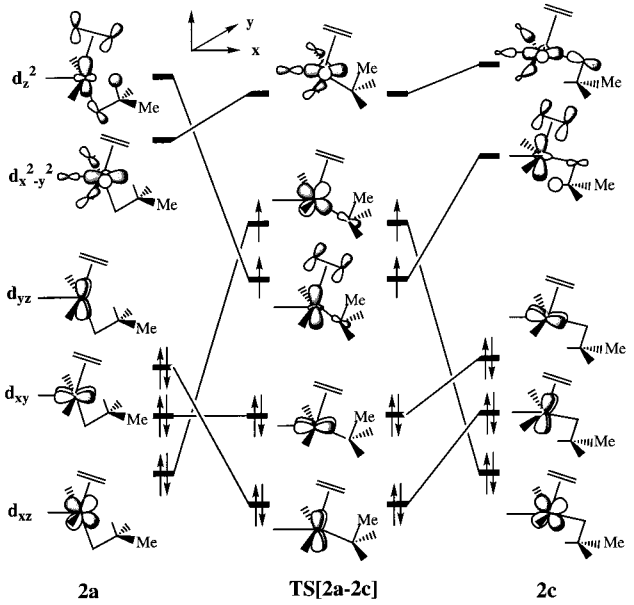

Figure 3. Schematic correlation diagram for the interconversion of the "axial" alkyl ethylene complex **2a** into the "equatorial" ethylene complex **2c**.

orbital (Figure 3) at **TS[2a−2c]**. The barrier can be lowered somewhat at **TS[2a−2c]** by adopting a triplet configuration in which one electron is promoted to the d_{z^2} orbital as it becomes stabilized by the movement of the C_α atom away from the axial site and the loss of the β-agostic bond, Figure 3. The barrier of interconversion is calculated to be 23.0 kcal/mol, Table 1. The ethylene complex **2c** can also be formed by addition of C_2H_4 anti (backside) to the β-H agostic bond of **1a** in an axial path from the same side of the iron−nitrogen plane as the C_α atom. This channel possesses a moderate barrier of 6.1 kcal/mol with the transition state lying on the triplet PES. The origin of this barrier is again the movement of C_α from the axial to the equatorial position.

We have finally located **2d** in which ethylene occupies an axial position with the propyl group situated in an equatorial

site. This conformer exhibits a weak α-H agostic interaction (Figure 2). The isomer **2d** is 14.9 kcal/mol above **2a** in energy**.** It can be formed by rotating the $C_\beta-H_\beta$ bond around the $C_\alpha-C_\beta$ axis of **2c**. The rotational barrier for this process is approximately 9 kcal/mol, i.e., the reverse process is nearly barrierless.

At normal catalytic conditions with a substantial monomer pressure, **2a** will be the predominant chain carrying species both in comparison to the alkyl complexes **1a**−**1d** without a coordinating monomer and the other alkyl complexes **2b**−**2d** with the monomer attached. Thus any productive chain propagation or chain termination step will have to start from this species.

iii. Chain Propagation. The direct ethylene insertion from the most stable π-complex **2a** gives rise to an insurmountable barrier (>40 kcal/mol) as the C_α atom has to move toward the equatorial plane to bind to the ethylene carbon. In doing so, the same repulsive interactions are encountered as in the **2a** to **2c** isomerization process, Figure 3. Insertion from the other "axial" π-complex **2b** is met with similar problems. Thus, the transition state **TS[2b**−**3b]** lies 37.3 kcal/mol above **2b**.

Ethylene insertion from the equatorial π-complexes **2c** and **2d** is on the other hand quite feasible as the C_α atom already is positioned in the equatorial plane. Thus, from **2c**, a transition state **TS[2c**−**3c]** with a barrier of 7.4 kcal/mol leads to an iron(II)−pentyl complex (**3c**) with a δ-agostic bond. The reaction enthalpy of this process is 0.6 kcal/mol, Table 1 and Figure 2. Another transition state **TS[2d**−**3d]** bears a resemblance to the complex **2d**. The corresponding product **3d** has a γ-agostic bond. The kinetic barrier of this path is only 0.9 kcal/mol, and its exothermicity is 9.5 kcal/mol.

We must conclude that direct insertion only is possible from the "equatorial" π-complexes **2c** and **2d**. However, insertion from the "equatorial" π-complexes would require a prior isomerization of the predominant π-complex **2a** to **2c** or **2d** since neither of the "equatorial" π-complexes would be present in appreciable concentrations. Such an isomerization will be associated with a large barrier (20−30 kcal/mol). Thus, chain propagation is not a facile process for the "generic" model system where ethylene after uptake will be stuck in the unreactive "axial" π-complex **2a**.

It is interesting to note that electron-poor d^0 $L_2MR(+)$ catalysts as well prefer a conformation with the C_α atom out of the L_2M coordination plane.[21,59] For these systems too the barrier of insertion is largely determined by the energy required to bring the C_α atom into the L_2M coordination plane.[20,59]

iv. Chain Termination and Isomerization. At low ethylene pressure the most stable alkyl complex **1a** might exist in sufficiently high concentrations for chain termination to take place by a β-hydrogen elimination mechanism, BHE of Figure 1. In the first step of this mechanism a β-hydrogen migrates to the metal center via a **1c**-like transition state **TS[1a**−**4a]** with a barrier of ca. 11.5 kcal/mol, Figure 2. This unimolecular elimination step is endothermic by 1.2 kcal/mol and leads to an iron(II)−propylene hydride complex **4a**. In the final step the polymer (propylene) is ejected from **4a** to form the separated species $Fe^{II}LH^+$ [(**5a**) or **5a(t)**] + C_3H_6. However, the ejection step requires about 37 kcal/mol, Figure 2, which makes the BHE mechanism unfeasible under the assumed low ethylene concentration where an incoming monomer is unlikely to assist in the ejection step.

The high ejection energy makes it instead possible for the polymer chain in **4a** to reinsert into the Fe(II)−H bond. This process can result in a chain isomerization to the Fe(II)−isopropyl complex **6a** if the vinyl-terminated chain rotates about the Fe(II)−vinyl bond before the reinsertion. The optimized transition state **TS[4a**−**6a]** for the isomerization process lies only 7.0 kcal/mol above **4a**, and the product **6a** is 1.5 kcal/mol lower in energy than **1a**.

The alkyl complex **1a** will not be present in a sufficient concentration at higher monomer pressure to contribute to chain termination. The predominant species containing the polymer chain will instead be **2a** from which chain termination is possible by a hydrogen transfer mechanism, BHT of Figure 1. The first step in this termination mechanism involves the transfer of a β-hydrogen on the propyl growing chain to the coordinated ethylene. The product is a iron(II)−propylene ethyl complex **7a** (Figure 2, left) that is 1.2 kcal/mol lower in energy than the reactant **2a**. The process has a low barrier of 4.0 kcal/mol and an almost symmetrical transition state **TS[2a**−**7a]** in which the $H_\beta-C_\alpha$(propyl) and H_β−C(ethyl) distances are 1.56 and 1.58 Å, respectively (Figure 2). The Fe(II)−H_β distance is only 1.56 Å at the TS, indicating that a strong metal assistance helps in reducing the activation energy of the β-hydrogen transfer. The final step in the termination mechanism is the ejection of the polymer chain (propylene) from **7a** to form the separated species **8a,** Figure 2. However, the ejection step requires 29.1 kcal/mol, Figure 2, which makes the BHT termination mechanism unlikely even if the required energy could be reduced from assistance by an incoming monomer. Termination by BHT is not likely to involve any of the other more energetic alkyl ethylene complexes **2b**, **2c**, and **2d** as their concentrations would be low. In addition, they do not have the right conformation for a facile and direct transfer of a β-hydrogen to olefin.

The propylene ethyl complex **7a** formed from β-hydrogen transfer can isomerize to **9a** by a 180° rotation of the propyl ligand. This process has a barrier of 3.3 kcal/mol and is slightly exothermic with a barrier of 4.8 kcal/mol for the reverse process. Finally a β-hydrogen transfer from ethyl to the propyl ligand results in an isopropyl ethylene π-complex **10a**, Figure 2. Neither of the olefin alkyl complexes **10a**, **9a**, and **7a** can undergo insertion more readily than **2a** since they all have the C_α atom in an axial position.

v. Catalytic Behavior of the Generic System for Ethylene Polymerization. We have found that the "generic" model for the Brookhart/Gibson catalyst, **1a**, readily binds ethylene to form the stable π-complex **2a**. However, **2a** cannot directly insert ethylene into the Fe−C_α bond. Instead **2a** has to convert to **2c** via **TS[2a**−**2c]** with a barrier of 23 kcal/mol. The high barrier of interconversion makes insertion unfeasible.

At monomer concentrations normal for polymerization, chain termination can only take place from **2a** via a hydrogen transfer mechanism, BHT of Figure 1. However the final step in the termination process requires the ejection of the polymer π-complexed to the metal center which has a high thermodynamic barrier of 29.1 kcal/mol. Thus, once **2a** is formed neither chain transfer nor propagation seems feasible. The only reaction path available for the thermodynamic sink **2a** is a series of isomerization processes to other olefin alkyl complexes (**10a**, **9a**, and **7a**) that are just as inert toward insertion and termination as **2a**.

B. The "Real" Systems. We shall in this section discuss the catalytic activity of the "real" Brookhart/Gibson system and the role played by the bulky phenyl substituents attached to the chelating nitrogen atoms. Table 2 collects relative energies and Figure 4 illustrates the corresponding energy profiles on the

(59) Margl, P. M.; Deng, L.; Ziegler, T. *Organometallics* **1998**, *17*, 933.

Table 2. Relative Energies (kcal/mol) of the Stationary Points on the Singlet Potential Energy Surface for the "Real" System

category	description	species	energy[a]	barrier/ enthalpy[b]
alkyl complex + C_2H_4	axial β-agostic	**1A**	0.0	
	axial nonagostic	**1B**	10.6	
	equatorial β-agostic	**1C**	15.9	
ethylene capture of alkyl complex	**1A**−C_2H_4 FS adduct	**2A′**	−4.5	
	1A−C_2H_4 BS adduct	**2C′**	−3.4	
	C_2H_4 FS attack TS	**TS[2A′−2A]**	4.5	9.0
	C_2H_4 BS attack TS	**TS[2C′−2C](t)**	3.7	7.1
π-complexes	FS β-agostic	**2A**	−8.4	
	nonagostic axial	**2B**	−13.4	
	BS β-agostic	**2C**	−6.2	
insertion TS	BS insertion TS	**TS[2C−3C]**	−5.9	0.3
insertion products	β-agostic	**3A**	−27.9	
	γ-agostic	**3D**	−26.1	
	δ-agostic	**3C**	−24.4	
	TS δ- to γ-agostic	**TS[3C−3D]**	−16.6	7.8
	TS γ- to β-agostic	**TS[3D−3A]**	−18.0	8.1
β-H elimination	transition state	**TS[1A−4A]**	16.1	16.1
	product	**4A**	9.8	
	chain-ejection products	**5A** + C_3H_6	42.3	32.5
	4A isomerization TS	**TS[4A−6A′]**	16.7	
β-H transfer	transition state	**TS[2A−7A]**	−3.9	4.6
	product	**7A**	−7.8	
	chain-ejection products	**8A** + C_3H_6	−0.6	

[a] Energies relative to **2A** + C_2H_4. [b] Reaction barrier and enthalpy relative to the direct processor.

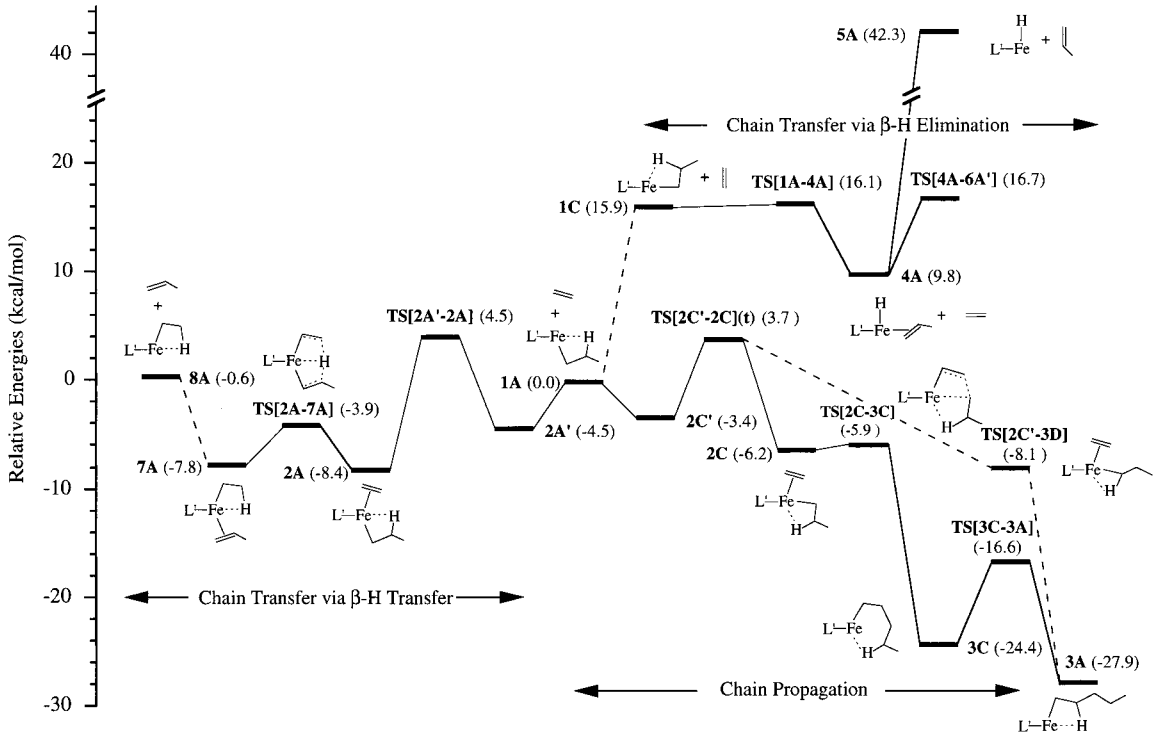

Figure 4. Singlet potential energy surface for "real" model system. TS[**2C'**−**2C**](t) situated on the triplet surface. Note that the iron−nitrogen coordination plane is perpendicular to the paper.

singlet PES. A brief discussion will also be provided of the possible role played by triplet and quintet species.

i. The Iron(II) Alkyl Complexes and Uptake of Ethylene Monomer. As for the model system, the "real" cationic iron(II) alkyl complex prefers a conformation with the C_α atom in an axial position and a β-agostic hydrogen attached to the metal, **1A** of Figure 5. The two conformational isomers **1B** and **1C** are calculated to be respectively 10.6 and 15.9 kcal/mol higher in energy.

We have located two ethylene complexes, **2A** and **2C**, that are readily accessible from the predominant cationic iron(II) alkyl complex **1A**. The frontside complex **2A** is formed by an attack of ethylene from above the iron(II) coordination plane trans to the C_α atom. The attack leads initially to an adduct **2A′** in which the incoming ethylene is loosely attached to the metal through van der Waal's attraction with the educt energy of −4.5 kcal/mol. When the ethylene approaches further to the metal center, it proceeds next through the transition state **TS[2A′−2A]**, Figure 6, with a barrier of 9.0 kcal/mol to form an ethylene π-complex **2A** in which the ethylene is more tightly coordinated to the metal center with the π-complexation energy being −8.4 kcal/mol. The axial coordination of C_α in **1A** enforces an orientation of the phenyl groups that blocks the approach of ethylene from above the iron−nitrogen coordination plane trans

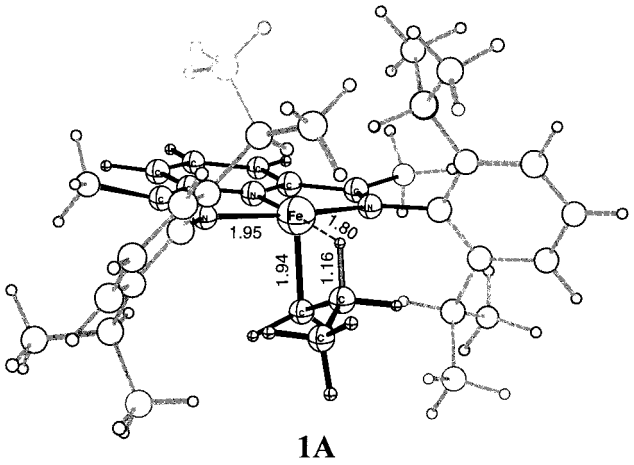

1A

Figure 5. Optimized structure for "real" cationic iron(II) alkyl complex **1A**. Note that path of ethylene from above iron−nitrogen coordination plane trans to C_α is blocked by the two (top) isopropyl groups on the aryl rings whereas the path cis to C_α is open. MM atoms are shaded for clarity. Distances shown are in angstroms. (Cartesian coordinates for all structures are provided in the Supporting Information.)

to C_α, and results in the large capture barrier of 9.0 kcal/mol. The same steric repulsion is further responsible for the modest ethylene complexation energy. Both the high barrier and the low stability are beneficial since **2A** can serve as a termination precursor. We note that ethylene uptake of the analogous model complex **1a** to form **2a** lacks an enthalpic barrier and gives rise to the stable complex **2a** with an ethylene binding energy of −29.7 kcal/mol, Figure 2.

The backside complex **2C** can be reached from an axial ethylene approach from the same side of the iron−nitrogen coordination plane as the C_α atom. This pass leads initially to the adduct **2C′** with an educt energy of −3.4 kcal/mol. The aduct **2C′** passes over the transition state **TS[2C′−2C](t)**, Figure 6, with a barrier of 7.1 kcal/mol to **2C** for which the ethylene complexation energy is −6.2 kcal/mol, Figure 4. The alkyl complex **1A** leaves plenty of room for **TS[2C′−2C](t)** to form without steric interference from the phenyl groups and their isopropyl substituents, Figures 5 and 6. The barrier associated with **TS[2C′−2C](t)** is instead electronic in nature and stems from the movement of the C_α atom from the axial to the equatorial position. This movement gives rise to a small HOMO/LUMO gap and a triplet transition state, as discussed previously in connection with the "generic" model system, Figure 3.

We have located a third ethylene complex (**2B)** on the singlet potential surfaces, Table 2. This complex lacks an agostic interaction and has C_α in an axial position. The steric destabilization is less severe for **2B** that has a favorable complexation energy of −13.3 kcal/mol, Figure 4. However, we have not been able to find a path to **2B** from the predominant cationic iron(II)−alkyl complex **1A** with a barrier below 15 kcal/mol, and as a consequence have not considered it as part of the catalytic cycle on the singlet PES.

In the generic system the frontside complex **2a** is the resting state for the alkyl chain, and serves as a thermodynamic sink from which it is difficult to reach other species on the catalytic polymerization cycle. By introducing steric bulk, the complexation energy for the frontside complex **2A** has been reduced (−8.4 kcal/mol) and the backside complex **2C** can now be formed from **1A** in competition with **2A**. In addition, on the free energy surface **1A** + C_2H_4 is now the resting state since entropy would add 10−15 kcal/mol to ΔG of ethylene complexation.[20] However, the precursors **2A** and **2C** for respectively chain termination and chain propagation will exist in (pre)-equilibrium with **1A**.

ii. Chain Termination and Chain Propagation. Insertion can proceed readily from **2C** through the transition state **TS-[2C−3C]**, Figure 6, with an insignificant barrier of 0.3 kcal/mol to form the kinetic polymerization product **3C** with a δ-agostic bond. Thus as **2C** is formed in equilibrium with **1A**, it will convert irreversibly to **3C** in a highly exothermic reaction of −18.2 kcal/mol, Figure 4. The thermodynamically more stable alkyl conformations with a β-agostic bond can finally be formed by rearrangement to complete the catalytic insertion cycle.

Termination by BHT, Figure 4 and Table 2, is not as favorable as insertion since it proceeds through the transition state **TS-[2A−7A]** with a barrier of 4.5 kcal/mol. Termination by BHE through the transition state **TS[1A−4A]** is even less favorable with a barrier of 16.1 kcal/mol, Figure 4. The high barrier of BHE inhibits as well chain isomerization through formation of **4A** followed by rotation of the vinylic chain and reinsertion into the Fe−H bond, Figure 4.

It follows from our discussion above that the rates of chain propagation and chain transfer are determined by the formation of the precursors **2A** and **2C** rather than the subsequent insertion and termination carried out by **2C** and **2A**, respectively. This aspect differs from ordinary d^0 catalyst as well as the Ni(II)/Pd(II) Brookhart[9,10] systems in which the actual insertion and termination is rate determining whereas ethylene capture is without an enthalpic barrier.

Experiment[7b] finds the rates of termination and insertion both to be first order in ethylene pressure for the iron(II) system. This is in agreement with our findings, and lends further credence to our suggestion that termination takes place by a bimolecular BHT rather than a unimolecular BHE. Our calculations do not favor a bimolecular termination process involving monomer-assisted BHE,[10] although such a mechanism would be consistent with experiment as well. Increasing steric bulk is seen to impede the formation of the termination precursor (**2A**) (and chain transfer) whereas insertion is less affected since the barrier to formation of the insertion precursor **2C** is electronic. It is thus not surprising that the molecular weight can be controlled experimentally[7b] from oligomers with methyls as substituents on the phenyl groups to polymers in the case of isopropyl substituents. We shall in the next section briefly discuss the shape of the termination and propagation energy profiles on the PES's of higher spin multiplicities.

iii. Higher Spin Potential Energy Surfaces. It is found experimentally[7,8] that the catalytic precursor [2,6-((2,6-C_6H_4(i-Pr))N═C(CH_3))$_2$−C_5H_3N]$FeCl_2$ has a quintet ground state. However, we find that the quintet state for active species such as **2a(q)**/**2A(q)** is well above the singlet ground state (15.5/18.2 kcal/mol). This is understandable since alkyl and ethylene groups exert a stronger "crystal" field than the two chlorine ligands. Nevertheless, we have for the sake of completeness carried out exploratory calculation for the quintet state.

The accessible conformations on the quintet PES are restricted to geometries with C_α in an axial position. The calculated barriers are 18.5 ("generic") and 20.6 kcal/mol ("real") for insertion compared to 27.5 ("generic") and >30 kcal/mol ("real") for termination. The high barriers are not unexpected[60] for a system with one or more electrons in each d orbital. We can conclude that it would be impossible for the polymerization processes to take place on the quintet PES. In fact, we speculate that the role of the third nitrogen on the tridentate ligand is to

(60) Schmid, R.; Ziegler, T. *Organometallics*, submitted for publication.

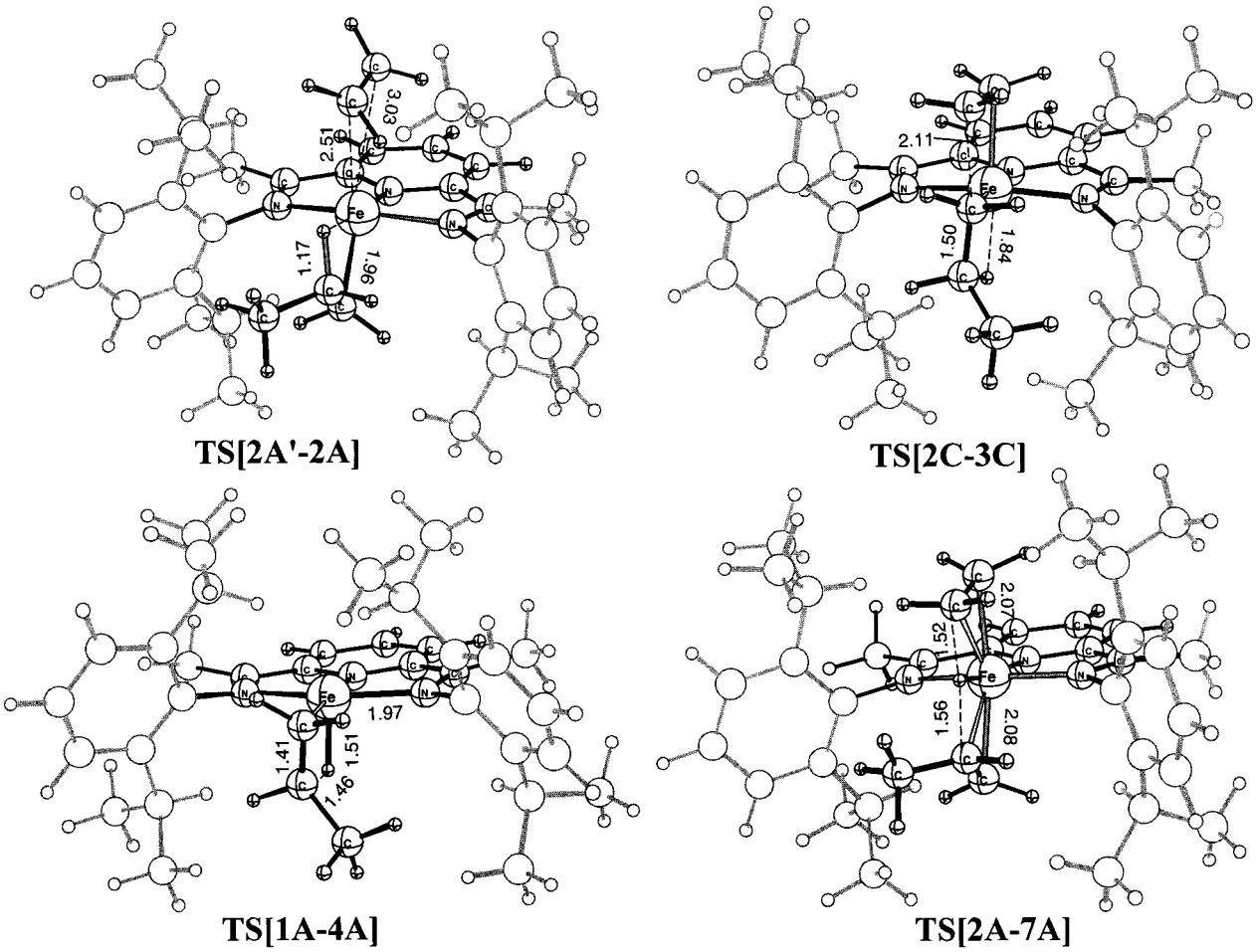

Figure 6. Transition state structures for the real system: TS[**2A'**−**2A**], frontside ethylene uptake TS; TS[2C−3C], backside insertion TS; TS-[**1A**−**4A**], the BHE TS; and TS[**2A**−**7A**], the BHT TS. Conventions as in Figure 5.

raise $d_{x^2-y^2}$ sufficiently in energy to destabilize quintet states for the species of importance in the catalytic cycle.

On the triplet PES, Figure 7, the insertion precursor is **2D(t)** and chain propagation has a barrier of 8.1 kcal/mol. The termination precursor **2A(t)** is 15.1 kcal/mol higher in energy than **2D(t)** and the barrier of termination is 7.5 kcal/mol. Estimates of energy separations between spin multiplets are difficult to determine with an accuracy of a few kilocalories/mole by any theoretical method, including DFT, and we expect BP86 used here to have a slight bias in favor of low spin[61] (singlet). Thus, the triplet transition state **TS[2C′−2C](t)** for the formation of the insertion precursor **2C** might actually be lower in energy relative to the singlet PES. We should thus consider the calculated barrier of 7.1 kcal/mol associated with the triplet transition state **TS[2C′−2C](t)** as an upper bound.

Concluding Remarks

We have presented an extensive theoretical study of the mechanisms for the new iron(II)-containing Brookhart/Gibson ethylene polymerization catalyst based on DFT and a combined DFT/MM (QM/MM) method.

The chain carrying the resting state for the new catalyst is a cationic iron(II)−alkyl complex rather than an ethylene complex as in the case of the Ni(II)− and Pd(II)−diimine polymerization catalysts previously designed by Brookhart[9,10] et al. We find that the cationic iron(II) alkyl resting state adopts a conformation with the C_α atom in an axial position above the iron−nitrogen coordination plane and a β-agostic hydrogen bound to the metal, **1A** of Figure 5. Both chain-propagation and chain-termination can proceed from the attack of ethylene on **1A**.

Chain propagation commences through the (backside) approach of ethylene from the same side of the iron−nitrogen coordination plane as C_α. This approach leads to an attack on the $C_\alpha-C_\beta$ bond of the alkyl group in **1A** to form a (BS) π-complex **2C** from which the insertion takes place with a modest barrier. The chain propagation is driven by a strong thermodynamic force with an exothermicity of 27.9 kcal/mol. The rate-determining step for the chain propagation is capture of ethylene by **1A** with an enthalpic barrier for which the upper bound is 7.1 kcal/mol.

The dominant chain termination (transfer) path is β-H transfer from the polymer chain to the incoming monomer. The rate-determining step in this process is capture of ethylene by **1A** to form the π-complex **2A** with an intrinsic activation energy of 9.0 kcal/mol. From **2A** β-H transfer can commence with an activation energy of 4.5 kcal/mol. Steric bulk helps suppress the formation of the termination precursor **2A** by introducing a capture barrier as ethylene encounters the repulsion of the isopropyl groups in its path toward the metal center from above the iron−nitrogen plane trans to C_α, Figures 5 and 6. Steric bulk has in addition the effect of destabilizing the ethylene complexation energy of **2A**. In the generic system the frontside complex **2a** serves as a thermodynamic sink (with an ethylene complexation energy of −29.7 kcal/mol) from which it is

(61) Jones, D. H.; Hinman, A. S.; Ziegler, T. *Inorg. Chem.* **1993**, 32, 2092−2095.

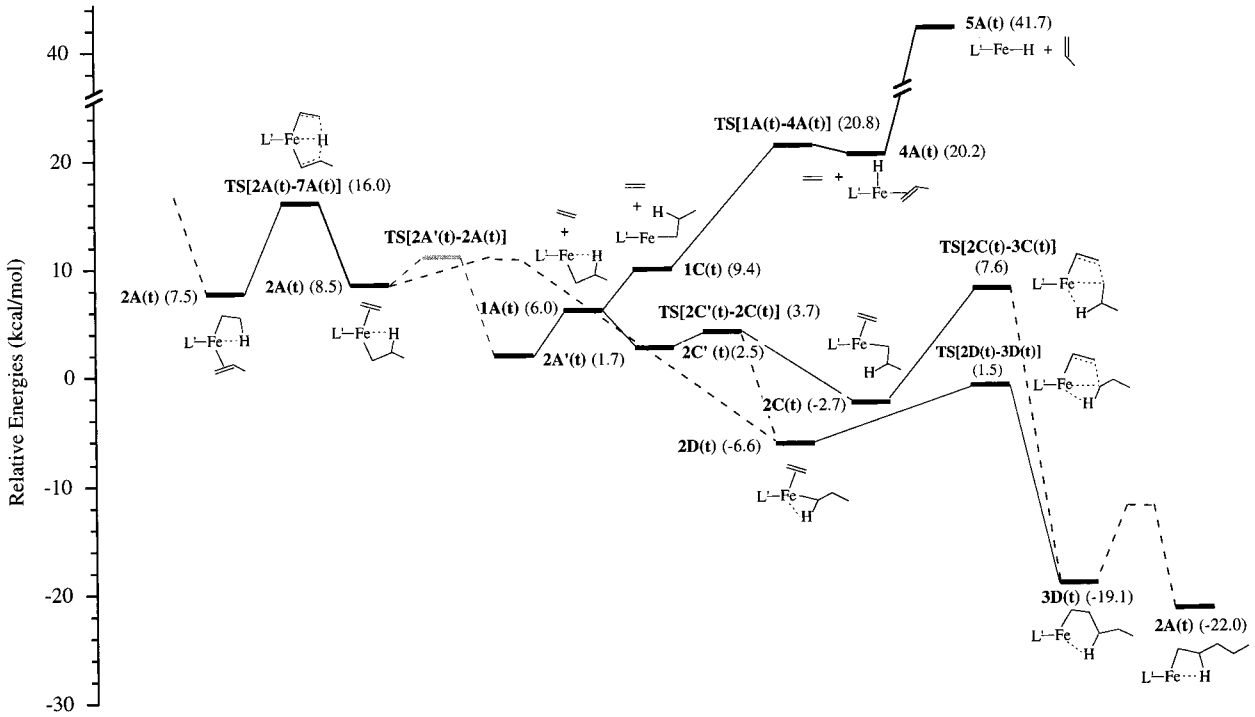

Figure 7. Triplet potential energy surface for "real" model system. Note that the iron−nitrogen coordination plane is perpendicular to the paper.

difficult to reach other species on the catalytic polymerization cycle. By introducing steric bulk, the complexation energy for the frontside complex **2A** has been reduced (−8.4 kcal/mol) and the backside complex **2C** (propagation precursor) can now be formed from **1A** in competition with **2A**.

We find that the quintet states for the chain-carrying intermediates are too high in energy compared to other multiplets to be of importance. Furthermore, both insertion and termination on the quintet PES are calculated to have prohibitively high barriers (20−30 kcal/mol). Our calculations place both the termination and propagation on the singlet surface. However, for propagation the singlet and triplet PES's are calculated to be close in energy with the crucial transition state **TS[2C′−2C](t)** for the formation of the insertion precursor (**2C**) on the triplet PES.

We predict ethylene capture by the cationic iron(II) alkyl complex **1A** to be rate determining for both termination and propagation with free energy of activations given by $\Delta G^{\neq}_{\mathrm{FS-capture}}$ and $\Delta G^{\neq}_{\mathrm{BS-capture}}$, respectively. In this picture molecular weights (M_w) can be estimated by

$$\begin{aligned}\Delta\Delta G^{\neq} &= \Delta G^{\neq}_{\mathrm{FS-capture}} - \Delta G^{\neq}_{\mathrm{BS-capture}} \\ &= [\Delta H^{\neq}_{\mathrm{FS-capture}} - \Delta H^{\neq}_{\mathrm{BS-capture}}] - \\ &\qquad T[\Delta S^{\neq}_{\mathrm{FS-capture}} - \Delta S^{\neq}_{\mathrm{BS-capture}}] \\ &\approx [\Delta E^{\neq}_{\mathrm{FS-capture}} - \Delta E^{\neq}_{\mathrm{BS-capture}}] - \\ &\qquad T[\Delta S^{\neq}_{\mathrm{FS-capture}} - \Delta S^{\neq}_{\mathrm{BS-capture}}] \quad (1)\end{aligned}$$

The $\Delta\Delta G^{\neq}$ values estimated from experimental M_w data[7,8] range from 4.0 to 6.0 kcal/mol. These values might be reconciled with our findings if we assume that the theoretical estimates for $\Delta E^{\neq}_{\mathrm{FS-capture}} - \Delta E^{\neq}_{\mathrm{BS-capture}}$ of 1.9 kcal/mol carry an error of 2−4 kcal/mol. This is not unreasonable since the barriers associated with BS and FS capture are respectively electronic and steric in nature. Thus, a cancellation of errors is less likely than if both barriers were caused by similar factors. In particular, we have argued that $\Delta E^{\neq}_{\mathrm{BS-capture}}$ might be a lower bound. Finally, one should also consider the contribution from $\Delta\Delta S^{\neq}$ to $\Delta\Delta G^{\neq}$. Both $\Delta S^{\neq}_{\mathrm{FS-capture}}$ and $\Delta S^{\neq}_{\mathrm{BS-capture}}$ would be negative and dominated by the reduction in the translation and rotational degrees of freedom of ethylene as this molecule is captured. However, superimposed on this could be a small difference that would contribute to $\Delta\Delta S^{\neq}$ and $\Delta\Delta G^{\neq}$. We do not feel that we are able at the moment to estimate this differential contribution with sufficient accuracy within the QM/MM methodology.

Acknowledgment. This investigation has been supported by the National Sciences and Engineering Research Council of Canada (NSERC) and by the donors of the Petroleum Research Fund, administered by the American Chemical Society (ACS-PRF No. 31205-AC3), as well as by Novacor Research and Technology Corporation (NRTC) of Calgary.

Supporting Information Available: Cartesian coordinates and total energy of all species mentioned in the text and a full listing of the molecular mechanics force field parameters utilized (PDF). This material is available free of charge via the Internet at http://pubs.acs.org.

JA984385L